Hindawi
Advances in Civil Engineering
Volume 2019, Article ID 7235656, 13 pages
https://doi.org/10.1155/2019/7235656

Research Article

Optimization Method for Solving the Reasonable Arch Axis of Long-Span CFST Arch Bridges

Xuesong Zhang,[1] Ningyi Liang,[1] Xiaohong Lu,[1] Anbang Gu,[1] and Jidong Shan[2]

[1]*School of Civil Engineering, Chongqing Jiaotong University, Chongqing 400074, China*
[2]*Ningbo Communications Planning Institute Co., Ltd., Ningbo 315192, China*

Correspondence should be addressed to Ningyi Liang; 1050612898@qq.com

Received 2 May 2019; Revised 19 July 2019; Accepted 24 July 2019; Published 21 August 2019

Academic Editor: Kirk Hatfield

With the continuous construction of 500 m concrete-filled steel-tube (CFST) arch bridges such as the Bosideng Yangtze River Bridge and the Hejiang Changjiang Highway Bridge, the deviation between the dead pressure line and the arch axis produced by extant arch axis optimization methods increases. Therefore, an arch axis optimization method for long-span CFST arch bridges with a truss section must be designed. Following the optimization of the truss arch axis, this study develops the minimum section eccentricity method that aims to optimize the arch axis of long-span CFST arch bridges. To minimize the main tube eccentricity of the truss arch, the bending moment of the main tubes is reduced by applying the main tube eccentricity method iteratively in a finite element model. Afterward, a smooth and reasonable arch axis is fitted by applying a cubic spline interpolation function in MATLAB. The entire optimization procedure is performed using the Bosideng Yangtze River Bridge as an example. Compared with that of optimal arch axis line types (e.g., parabola and catenary) and other traditional arch axes, the bending moment of main tubes optimized by the proposed method is substantially lower and more uniformly distributed along the arch axis span. The mechanical properties of the finished bridge, including its strength, stiffness, and stability, are all improved, thereby verifying the feasibility of using the proposed method to optimize the arch axis of CFST arch bridges with a truss section.

1. Introduction

Given their use of concrete-filled steel tubular (CFST) materials and convenient construction, CFST arch bridges have been constructed on a large scale all across China. Long-span CFST arch bridges have also been built in the country given the mature calculation theory and construction technologies used by these structures. The truss section, also known as the truss arch, serves as the main arch section of long-span CFST arch bridges. Each CSFT bridge has a unique structural form and faces an increasingly complex stress state. Apart from the geometric nonlinearity of these bridges, the deviation between their arch bridge axis and pressure line increases as the latter moves toward a circular curve, parabola, and catenary with few control parameters, which are unable to meet the structural force requirements. Therefore, to ensure a reasonable stress state for the truss arch of long-span CFST arch bridges, a reasonable arch axis must be selected [1–4].

Arcs, parabolas, catenaries, and spline curves are generally selected as arch axes of arch bridges. Arcs are derived from hydrostatic pressure lines and show huge deviations from the true dead load pressure line of an arch bridge, thereby making them applicable only to small arch bridges spanning less than 20 m. Quadratic parabolas are derived from three-hinged arches under the action of vertical uniform load. Give that the load on a CFST arch bridge is lighter than that on a masonry arch bridge (which is close to the vertical uniform load), most CFST arch bridges spanning less than 100 m use parabolas as their arch axes. Catenaries, which are used by most long-span CFST arch bridges [5], are derived from the dead load pressure of full-web arch bridges. These three axes also determine the arch axis shape of an arch bridge by using very few linear parameters, thereby

explaining why most information related to the design of long-span arch bridges is not disclosed [6–9]. Therefore, scholars have proposed spline interpolation function to fit and approximate the dead load pressure line in the optimization design of arch axes [10–14]. To make the design of the arch axis as close as possible to that of the dead load pressure line, the selected arch axes need to be optimized by applying an optimization method. For instance, to minimize the deviation between the arch axis and load pressure line of a small-span catenary arch bridge, the five-point coincidence method must be applied to determine the arch axis coefficient of the catenary. However, each calculation relies on the table data in the "Arch Bridge," thereby leading to a cumbersome and inefficient calculation process. This calculation method is suitable for CFST arch bridges with a single tube section, while for CFST arch bridges with dumbbell and truss arches, the characteristics of their key sections must be calculated manually, thereby leading to low calculation efficiency [15]. For long-span CFST arch bridges, scholars have introduced the minimum bending energy method [16], which has been widely used in optimizing the cable force of cable-stayed bridges. Zhou and Li proposed a multiparameter arch axis optimization method based on the deformation energy of the arch axis and used the spline curve to approximate the pressure line of the main arch ring [17]. Hou and Song used the minimum bending energy method to optimize the arch axis coefficient based on APDL language and used the global optimization algorithm to find the optimal solution of the arch axis coefficient [18]. In general, the minimum bending energy method considers the deformation energy generated by the structural bending moment yet ignores the contribution of shear force to the deformation energy. Therefore, this method may generate some errors for CFST arch bridges with many main and branch tubes. Although the total bending moment energy of the main arch rib of a CFST arch bridge can be minimized, the local bending moment of the main arch rib at the arch foot section and border of the arch girder section is not considered, thereby destroying the main arch rib in case of an excessive local bending moment. Other scholars have proposed the minimum section eccentricity method, which controls the bending moment of the main arch rib by controlling the deviation between the arch axis and dead load pressure line. Xu and Shen used this method along with the cubic spline interpolation to fit the arch axis [19, 20]. Despite minimizing the bending moment of the whole control section, the minimum section eccentricity method cannot optimize the stress state of the main tubes in the section [21]. Similar to the five-point coincidence method, the characteristics of the key sections of dumbbell and truss arches must be calculated manually.

Optimizing the main truss of long-span CFST arch bridges ensures that the main tubes of the truss section are in an optimal stress state. To this end, this paper proposes the minimum main tube eccentricity method as a new optimization method specifically designed for arch axes. A finite element model has also been established to treat the initial stress state of the whole structural system as the initial state of geometrically nonlinear calculation [22, 23]. To minimize the main tube eccentricity of the truss arch, the relationship between the bending moment of the main tube and the adjustment value of main tube eccentricity is established, and the maximum main tube eccentricity of each truss section is iterated to the admissible value range [24] by changing the vertical coordinates of the main tubes of each truss section. The cubic spline function is then applied to interpolate and fit a smooth curve to facilitate the construction [25, 26]. This method does not require users to consult table data and manually calculate the characteristics of key sections. Instead, this formula focuses on optimizing the configuration of the truss arch without optimizing the cable and floor systems. Such assumption seems reasonable, especially given that the stress state of a long-span arch bridge greatly depends on the characteristics of the arch axis and that the cable system plays a key role in load transmission.

The rest of this paper is outlined as follows. Section 2 formulates the relationship between main tube bending moment and main tube eccentricity adjustment and presents the initial configuration of the finite element model, the main tube eccentricity iteration process, and the cubic spline curve interpolation fitting process. Section 3 discusses the optimization of the truss arch of the Bosideng Yangtze River Bridge. Section 4 presents some interesting conclusions about this new optimization method.

2. Theoretical Derivation of the Minimum Main Tube Eccentricity Method

2.1. Concept of the Minimum Main Tube Eccentricity Method. Among the members of a truss arch, main tubes bear the axial pressure along the arch axis, whereas branch tubes connect and support the main tubes while bearing the shear force and a small amount of axial force in the whole truss beam element. Therefore, when optimizing the arch axis of a truss arch, only the bending moment of main tubes needs to be considered to ensure a minimum bending moment under a dead load. To minimize the main tube eccentricity of a truss arch and subsequently optimize the arch axis of a CFST arch bridge, the maximum main tube eccentricity of each truss section should be reduced.

Following the internal force and parameters of each member as illustrated in Figures 1 and 2, the main tube eccentricity of truss section can be calculated as

$$e_{ij} = \frac{M_{ij}}{N_{ij}}, \quad i = 1, 2, \ldots, n;\ j = 1, 2, \ldots, m, \tag{1}$$

where N_{ij} denotes the designed axial force value of main tube j at section i, M_{ij} denotes the designed bending moment value of main tube j at section i, n denotes the total number of truss sections, and m is the total number of main tubes of each truss section ($m = 8$).

The main tube eccentricity of section i can be calculated as

$$E_i = \max\{e_{i1}, e_{i2}, \ldots, e_{im}\}, \tag{2}$$

where m is the number of main tubes of each truss section.

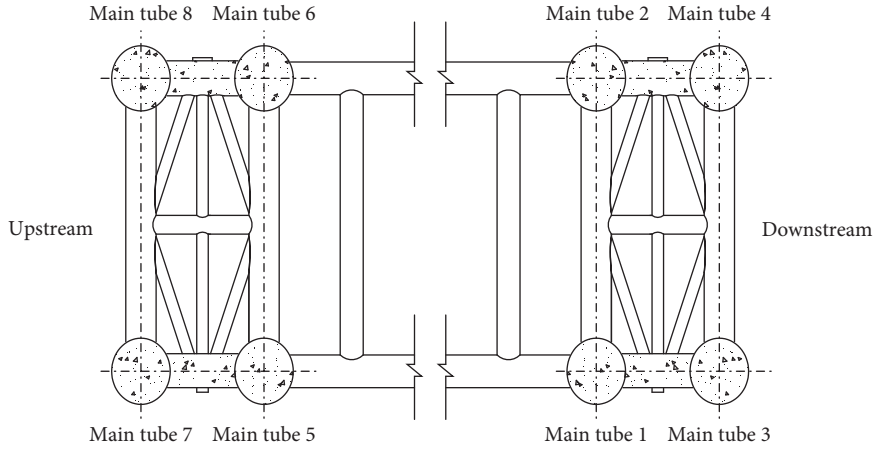

Figure 1: Schematic of the truss section.

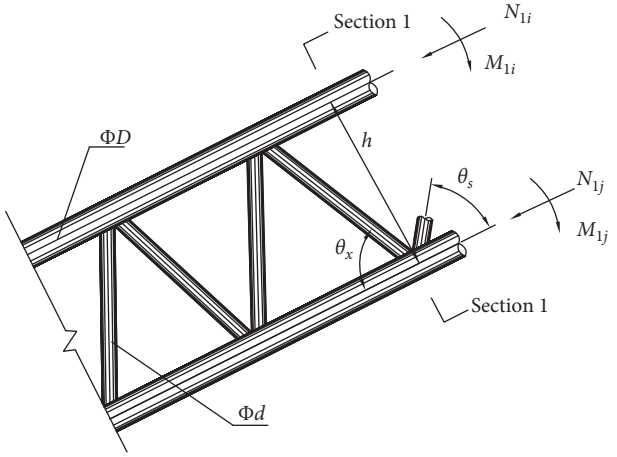

Figure 2: Schematic of truss arch elevation.

$$E = \max\{E_1, E_2, \ldots, E_n\}. \tag{3}$$

Therefore, to minimize E and to obtain a reasonable arch axis for long-span CFST arch bridges, the main tube eccentricity of the truss section must be minimized.

2.2. Iterative Calculation of Main Tube Eccentricity. To minimize the main tube eccentricity of the truss arch, the optimization of the arch axis of a long-span CFST arch bridge needs to be analyzed. Given the complex structure of a truss arch and the uncertainty of arch axis shape, one cannot directly establish a relationship between the variations in main tube eccentricity and bending moment. Therefore, the truss arch design should be optimized by iterating the maximum main tube eccentricity of each truss section to an admissible value range [27, 28].

The following assumptions are established in the calculation:

(1) According to the characteristics of the discrete structure and by assuming that the length of two adjacent main tube elements l_i and l_j is infinitesimal, the internal force values of these elements, which are also treated as bar elements, are linearly distributed

(2) The total bending stiffness EI of the two adjacent elements is assumed to be constant, and the bending stiffness of node k is set to E_kI_k (where N_k denotes the intermediate arbitrary node of adjacent main tube elements l_i and l_j)

(3) The two adjacent main tube elements l_i and l_j are assumed to be associated with other adjacent main tube elements

Figure 3 shows a simplified calculation model, where l_i denotes the length of element E_i, l_j denotes the length of element E_j, and α denotes the angle between the main tube and horizontal line.

The bending moment M_k of node N_k can be formulated as

$$M_k = \frac{M_j - M_i}{l_i + l_j} \times l_i + M_i = \frac{M_j l_i + M_i l_j}{l_i + l_j}. \tag{4}$$

When forced displacement Δ_k is applied at node N_k, the bending moment at node N_k can be partially offset and Δ_k can be considered the adjustment value of main tube eccentricity. Applying Δ_k at node N_k is equivalent to applying concentrated force F_k.

$$\begin{aligned}\Delta_k &= \int \frac{M_k M_{pk}}{E_k I_k} ds = \frac{\sum A_i y_{0i}}{E_k I_k} \\ &= \frac{1}{E_k I_k}\left[\frac{1}{3}\frac{l_i^3 l_j^2}{\left(l_i + l_j\right)^2} F_k \cos^3\alpha + \frac{1}{3}\frac{l_i^2 l_j^3}{\left(l_i + l_j\right)^2} F_k \cos^3\alpha\right] \\ &= \frac{1}{3E_k I_k}\frac{l_i^2 l_j^2}{l_i + l_j} F_k \cos^3\alpha.\end{aligned} \tag{5}$$

The bending moment at node N_k can be calculated as

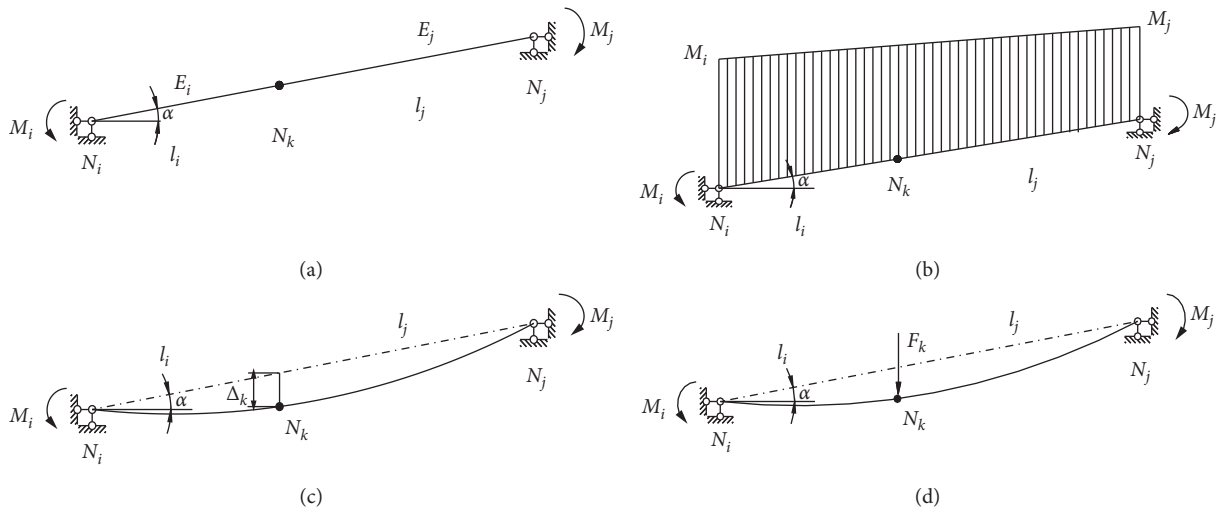

Figure 3: Simplified calculation model of the main tube. (a) Simplified structural diagram of the main tube. (b) Simplified bending moment diagram of the main tube. (c) Adjustment value Δ_k of node N_k. (d) Equivalent concentrating force F_k of node N_k.

$$M_k = \frac{l_i l_j}{l_i + l_j} F_k \cos\alpha. \tag{6}$$

By substituting formula (6) into formula (5), the following expression can be derived:

$$\Delta_k = \frac{1}{3E_k I_k} \frac{l_i^2 l_j^2}{l_i + l_j} \cos^3\alpha \times \frac{l_i + l_j}{l_i l_j \cos\alpha} M_k = \frac{l_i l_j}{3E_k I_k} M_k \cos^2\alpha. \tag{7}$$

The deviation coefficient of main tube eccentricity (ξ_Δ) is then derived to represent the convergence rate of the main tube eccentricity of each truss section. The adjustment value Δ_k of main tube eccentricity obtained by formula (7) is multiplied by the deviation coefficient ξ_Δ of main tube eccentricity, which is equivalent to the adjustment value Δ_{kk} of main tube eccentricity of each truss section in the current iteration. Such adjustment value and deviation coefficient can be computed as

$$\Delta_{kk} = \xi_\Delta \Delta_k = \frac{l_i l_j}{3E_k I_k} \xi_\Delta M_k \cos^2\alpha, \tag{8}$$

$$\xi_\Delta = \frac{E_i}{E_a}, \tag{9}$$

where E_i is the maximum main tube eccentricity of each truss section and E_a is the admissible value of the main tube eccentricity of the truss section.

Using these formulas, the adjustment value of main tube eccentricity for offsetting the bending moment at node N_k can be calculated.

2.3. Initial Configuration of the Finite Element Model. Given that the elements of a cable system require posttensioning forces, their initial configuration under dead loading must be identified in advance. To calculate the initial stress in each cable, the cable optimization model and constrained expression are built based on the cable force optimization and constrained energy minimization methods for a cable-stayed bridge [29]. Specifically, the optimum stress state of the structure is achieved by changing the posttensioning forces in the cable under the condition that the bridge structure system has been formed. The objective function can be formulated as

$$P = \int \frac{M^2(l)}{2E(l)I(l)} + \frac{N^2(l)}{2E(l)I(l)} dl, \tag{10}$$

where P is the sum of strain energy, E is the modulus of elasticity, I is the moment of inertia, M and N are the bending moment and axial force, respectively, and L is the design variable. Using the mathematical model of the quadratic programming method, the constrained objective function can be expressed as

$$\begin{aligned} &\min \quad f(t) = \frac{1}{2}\{t\}^T [K]\{t\} + [F]\{t\} \\ &\text{s.t.} \quad \{a \le t \le b;\ A \cdot t \le B;\ A\text{eq} \cdot t \le B\text{eq}\}, \end{aligned} \tag{11}$$

where $f(t)$ is the objective function of optimization, $[F]$ is the first-order coefficient array of t, $[K]$ is the second-order coefficient array of t, $[F]$ and $[K]$ are matrices comprising bending strain energy and tension-compression strain energy that are generated by structural elements during the optimization of posttensioning forces in the cable, A and Aeq denote the corresponding influence matrices of the posttensioning forces in the cable, B and Beq are the constraints, and $\{a\}$ and $\{b\}$ are the upper and lower bounds of $\{t\}$, respectively. MATLAB addresses the quadratic programming problem by solving the KT equation.

Given that a nonlinear behavior is expected, the cable system is simulated by the "cable element" instead of the "truss element" in the Midas finite element model. The initial tension of each cable leads to the initial stiffness of the elements of the cable system and the initial stress of the whole

structure system, thereby facilitating a geometric nonlinear analysis. In the finite element model analysis, the coupling behavior between the cable and floor systems leads to each cable not in the vertical direction, and the section stiffness of the cable element is modified in time according to the current tension of the cable element. The corner of nodes at both ends of the cable element represents the rotation angle of the tangent coordinate direction of the catenary element node, which is usually inconsistent with each other. The above finite element simulation reflects reality as close as possible.

2.4. Iterative Process of Main Tube Eccentricity. The iterative process of main tube eccentricity is illustrated in Figure 4.

Step 1. The initial state of a long-span CFST arch bridge is calculated by tentatively defining an arch axis (e.g., quadratic parabola or catenary), which is set to Ml_0.

Step 2. The maximum bending moment M_0 of each truss section in the initial state of the structure is extracted and defined as Ml_0, where $M_0 = \{M_{01}, M_{02}, \ldots, M_{0n}\}$ and $M_{0i} = \mathrm{Max}\{M_{011}, M_{012}, \ldots, M_{01m}\}$. By using formula (8), the adjustment values Δ_{kk} of the maximum main tube eccentricity of each truss section are calculated, where $\Delta_{kk} = \{\Delta_{k1}, \Delta_{k2}, \ldots, \Delta_{kn}\}$, $\Delta_{ki} = \mathrm{Max}\{\Delta_{k11}, \Delta_{k12}, \ldots, \Delta_{k1m}\}$, n is the total number of truss sections, and m is the total number of main tubes of each truss section ($m = 8$).

Step 3. The coordinate value Z of each truss section node in the initial state of the structure is extracted, where $Z = \{Z_1, Z_2, \ldots, Z_n\}$ and $Z' = Z - \Delta_k$.

Step 4. In the finite element model, the calculated coordinates Z' of the truss arch element nodes are used instead of the original coordinates Z to obtain the updated structural state Ml_1 and to perform a structural calculation.

Step 5. The bending moments and axial forces of the truss arch elements in structural state Ml_1 are extracted. Afterward, the maximum main tube eccentricity of the truss section is calculated using formulas (1) to (3), where $E(Z') = \mathrm{Max}\{E_1(Z'), E_2(Z'), \ldots, E_n(Z')\}$.

Step 6. The maximum main tube eccentricity $E(Z')$ is compared with the admissible value E_a of main tube eccentricity. If $E(Z') \le E_a$, then the main tube eccentricity iteration ends and moves to the next optimization step; otherwise, Steps 2 to 6 are repeated until $E(Z') \le E_a$ is satisfied.

2.5. Iterative Process of Simulated Annealing Algorithm. The simulated annealing algorithm is chosen to avoid trapping in local optima, which can not only iterate in the direction of objective function optimization but also accept the deterioration of objective function with a certain probability to ensure the reliability of obtaining global optimal solution [30–32].

The objective function which we set in MATLAB is as follows:

$$E(Z_*) = \min E(Z'), \tag{12}$$

where Z_* is the global optimal solution and Z' is the coordinate value of each truss section node. Then, we set the starting temperature T_0, the cooling rate parameter a, and the number of iterations of the inner loop L in advance. The specific steps of the iterative process of simulated annealing algorithm which searches for the minimum of the objective function can be described as follows:

Step 1 (initialization). The initial temperature T_0 and the initial solution Z_0' are set, and the objective function value $E(Z_0')$ corresponding to the initial solution Z_0' is calculated. The number of iterations per T_i is L.

Step 2. The internal loop iteration of steps 3 to 6 for $k = 1, 2, \ldots, L-1, L$.

Step 3. A new solution is generated by random variation in a certain neighborhood, $Z'_{i+1} = Z'_i \pm r^* \mathrm{scale}$, where $r \in (0, 1)$. This scale is an adaptive neighborhood factor which has a great influence on the optimization calculation, $(\mathrm{scale})_{i+1} = b * (\mathrm{scale})_i$, where $b \in (0, 1)$.

Step 4. Calculate the change $\Delta E = E(Z'_*) - E(Z)$, where ΔE is an evaluation function.

Step 5. If $\Delta E < 0$, then Z'_* is accepted as a new current solution. Otherwise, if $\Delta E > 0$ and $\exp(-\Delta E/T_i) > \mathrm{around}(0, 1)$, then Z'_* is accepted as a new current solution by the probability $\exp(-\Delta E/T_i)$; otherwise, the previous solution remains unchanged.

Step 6. If the termination condition is satisfied, the current solution is output as the optimal solution; otherwise, Step 7 is not allowed until the number of iterations of the inner loop $k \ge L$.

Step 7. T_i gradually decreases, $T_{i+1} = aT_i$, where $a \in (0, 1)$; then, turn to Step 2.

Then, a MATLAB program is presented to search for the minimum of the objective function using simulated annealing algorithm.

2.6. Interpolation and Fitting of the Arch Axis by Using the Cubic Spline Interpolation Function. The iterative calculation of main tube eccentricity produces an irregular arch axis instead of a smooth curve to guide construction. To ensure the curvature aesthetics and constructability of the arch axis, the cubic spline curve is used for interpolating and fitting this axis.

2.6.1. Derivation of the Coefficient Matrix A of the Cubic Spline Curve. According to the properties of the cubic spline curve, the second derivative $S''(x)$ of $S(x)$ is a linear function in each interval x_j, x_{j+1}. Assuming that $S''(x)$ is represented by M in each interval x_j, x_{j+1}, the following formula is introduced:

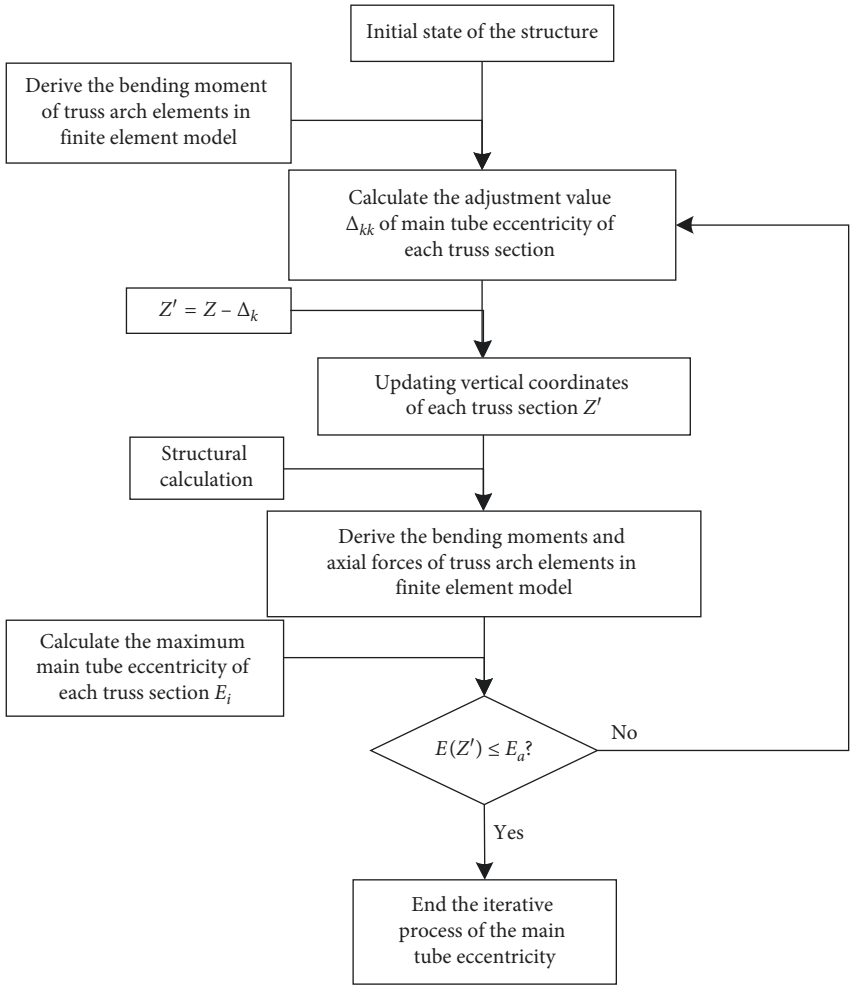

Figure 4: Iterative process of main tube eccentricity.

$$S''\left(x_j\right) = M_j \frac{x_{j+1} - x}{h_j} + M_{j+1} \frac{x - x_j}{h_j}. \tag{13}$$

By integrating formula (13) twice and introducing conditions $S(x_j) = y_j$ and $S(x_{j+1}) = y_{j+1}$, the following definite integral formula can be derived to represent the cubic spline interpolation function:

$$\begin{aligned} S(x) = {} & M_j \frac{\left(x_{j+1} - x\right)^3}{6h_j} + M_{j+1} \frac{\left(x - x_j\right)^3}{6h_j} \\ & + \left(y_j - \frac{M_j h_j^2}{6}\right)\left(\frac{x_{j+1} - x}{h_j}\right) \\ & + \left(y_{j+1} - \frac{M_{j+1} h_j^2}{6}\right)\left(\frac{x - x_j}{h_j}\right), \quad j = 1, 2, \ldots, n, \end{aligned} \tag{14}$$

which can be simplified as

$$S_j(x) = a_j x^3 + b_j x^2 + c_j x + d_j, \quad j = 1, 2, \ldots, n. \tag{15}$$

The polynomial coefficients a_j, b_j, c_j, and d_j are computed as

$$\begin{cases} a_j = \dfrac{1}{6h_j}\left(M_{j+1} - M_j\right), \\ b_j = \dfrac{1}{2h_j}\left(M_{j+1} x_j - M_j x_{j+1}\right), \\ c_j = \dfrac{1}{6h_j}\left[3\left(M_{j+1} x_j^2 - M_j x_{j+1}^2\right) + 6\left(y_{j+1} - y_j\right) + \left(M_j - M_{j+1}\right) h_j^2\right], \\ d_j = \dfrac{1}{6h_j}\left[\left(M_j x_{j+1}^3 - M_{j+1} x_j^3\right) + 6\left(x_{j+1} y_j - x_j y_{j+1}\right) + \left(M_{j+1} x_j - M_j x_{j+1}\right) h_j^2\right], \\ j = 1, 2, \ldots, n, \end{cases} \tag{16}$$

which can be transformed into the spline curve coefficient matrix A as

$$A = \begin{pmatrix} a_1 & b_1 & c_1 & d_1 \\ a_2 & b_2 & c_2 & d_2 \\ \vdots & \vdots & \vdots & \vdots \\ a_n & b_n & c_n & d_n \end{pmatrix}. \quad (17)$$

This research mainly focuses on the cubic spline curve interpolation fitting of the arch axis of a long-span CFST arch bridge. A half-bridge is selected as the interpolation fitting object due to the longitudinal symmetry of a CFST arch bridge. To ensure that the curvature at the midspan and arch foot of the CFST arch bridge remains unchanged, the first boundary condition of the cubic spline interpolation function is selected for the design, that is,

$$S'(x_1) = f'(x_1), S'(x_n) = f'(x_n), \quad (18)$$

where $f(x_1)$ and $f(x_n)$ are the slopes of the arch axis at the foot and midspan of a CFST arch bridge, respectively. Based on the longitudinal symmetry of the arch axis and the continuity of the second derivative, $f(x_n) = 0$.

2.6.2. Solving M_j. According to formulas (16) and (17), the spline curve coefficient matrix A can be obtained by determining M_j. The trigonometric equations of $M_j (j = 1, 2, \ldots, n)$ can be obtained by combining the boundary condition (19) as follows:

(1) Following the second-order continuity of the cubic spline curve at the nodes, $S(x)$ is derived by using $S'(x_j + 0) = S'(x_j - 0)$, that is,

$$S'(x) = -M_j \frac{(x_{j+1} - x)^2}{2h_j} + M_{j+1} \frac{(x - x_j)^2}{2h_j} + \frac{y_{j+1} - y}{h_j} - \frac{M_{j+1} - M_j}{6} h_j. \quad (19)$$

Therefore, the expression $S(x)$ on interval $[x_j, x_{j+1}]$ can be derived as

$$S'(x + 0) = -\frac{h_j}{3} M_j - \frac{h_j}{6} M_{j+1} + \frac{y_{j+1} - y}{h_j}, \quad (20)$$

whereas that on interval $[x_{j-1}, x_j]$ can be derived as

$$S'(x_j - 0) = -\frac{h_{j-1}}{6} M_{j-1} - \frac{h_{j-1}}{3} M_j + \frac{y_j - y_{j-1}}{h_{j-1}}. \quad (21)$$

Therefore, by using $S'(x_j + 0) = S'(x_j - 0)$,

$$\mu_j M_{j+1} + 2M_j + \lambda_j M_{j+1} = d_j, \quad j = 1, 2, \ldots, n - 1, \quad (22)$$

$$\mu_j = \frac{h_{j-1}}{h_{j-1} + h_j}, \lambda_j = \frac{h_j}{h_{j-1} + h_j}, \quad j = 1, 2, \ldots, n - 1, \quad (23)$$

$$d_j = 6 \frac{f[x_j, x_{j+1}] - f[x_{j-1}, x_j]}{h_{j-1} + h_j} = 6 f[x_{j-1}, x_j, x_{j+1}]. \quad (24)$$

(2) The formula is derived by using the first boundary condition.

By using formula (18), the following boundary condition can be obtained:

$$2M_0 + M_1 = \frac{6}{h_0} (f[x_0, x_1] - f'_0),$$
$$M_{n-1} + 2M_n = \frac{6}{h_{n-1}} (f'_n - f[x_{n-1}, x_n]). \quad (25)$$

(3) The equation group of M_j is solved.

Let $\lambda_0 = 1, d_0 = 6/h_0 (f[x_0, x_1] - f'_0)$, and $\mu_n = 1, d_n = 6/h_{n-1} (f'_n - f[x_{n-1}, x_n])$. Then, formula (25) can be written in the matrix form as

$$\begin{pmatrix} 2 & \lambda_0 & & & \\ \mu_1 & 2 & \lambda_1 & & \\ & \vdots & \vdots & \vdots & \\ & & \mu_{n-1} & 2 & \lambda_{n-1} \\ & & & \mu_n & 2 \end{pmatrix} \begin{pmatrix} M_0 \\ M_1 \\ \vdots \\ M_{n-1} \\ M_n \end{pmatrix} = \begin{pmatrix} d_0 \\ d_1 \\ \vdots \\ d_{n-1} \\ d_n \end{pmatrix}. \quad (26)$$

2.6.3. Calculation of the Cubic Spline Interpolation Function. Using formula (27), $M_j (j = 1, 2, \ldots, n)$ can be obtained. Meanwhile, by substituting $M_j (j = 1, 2, \ldots, n)$ into formula (17), the coefficient matrix A of the spline curve, which is the solution of the cubic spline interpolation function, can be derived.

The optimization process of the cubic spline interpolation function is shown in Figure 5.

Step 1. The M key sections, such as arch foot, quadrant, and midspan, of the arch axis curve of a CFST arch bridge after the last iteration are selected.

Step 2. The centroid coordinate $[X_g, Z_g]$ of the key sections of the truss arch is calculated, and $X_g = \{X_{g1}, X_{g2}, \ldots, X_{gm}\}$ and $Z_g = \{Z_{g1}, Z_{g2}, \ldots, Z_{gm}\}$. Given that the optimization of the truss arch does not involve transverse coordinates, the calculation does not consider the Y coordinates of nodes.

Step 3. In accordance with the theory and method of cubic spline interpolation function, the coefficient matrix A of the spline curve is calculated using MATLAB.

Step 4. In accordance with the method for calculating the parametric coordinates of the truss section, the coordinates of the nodes are modified by the circulating sentence in MATLAB, and the coordinates $[X, Z]$ of each node of the truss arch are obtained, where $X = \{X_1, X_2, \ldots, X_n\}$ and $Z = \{Z_1, Z_2, \ldots, Z_n\}$.

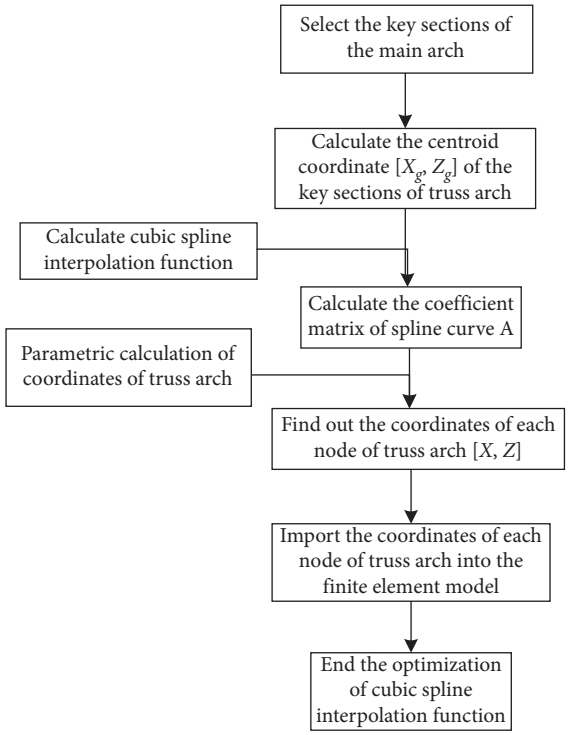

Figure 5: Optimization of the cubic spline interpolation function.

Step 5. The coordinate $[X, Z]$ of each node is introduced into the finite element model of the CFST arch bridge, and the optimization of the cubic spline interpolation function is completed.

3. Engineering Application

The iterative main tube eccentricity method, which considers the optimization of the cubic spline interpolation function, is used to optimize the truss arch of the 530 m Bodiseng Yangtze River Bridge as an example. The structural stress states before and after the optimization of the truss arch are also compared.

3.1. General Situation of the Bosideng Yangtze River Bridge. As shown in Figure 6, the main Bosideng Yangtze River Bridge is a half-through CFST arch bridge with a single span of 530 m. The load grade of the main bridge is highway class I. The width of the bridge deck is $2 \times 10.75\,\text{m} + 2 \times 1.75\,\text{m} + 2 \times 0.5\,\text{m} + 2\,\text{m}$, whereas its full width is 28 m. The main arch rib adopts a CFST truss structure with a 1/4.5 rise-to-span ratio and 1.45 arch axis coefficient. The cross-section height of the main arch rib gradually increases from the arch vault to the arch foot. The cross-section diameter of the arch vault is 8.0 m, whereas that of the arch foot is 16 m. The truss section comprises two CFST chords filled with C60 concrete, and the width of the main arch rib is 4.0 m. The transverse center distance of the two main chords is 2.68 m. The thickness of the main chord steel tube ($\varphi 1320 \times 22$ (26, 30, and 34) mm) gradually increases from the arch vault top to the arch foot.

3.2. Iterative Calculation of the Truss Arch of the Bosideng Yangtze River Bridge. Given that the arch axis of the Bosideng Yangtze River Bridge is a catenary with an arch axis coefficient of $m = 1.45$, the main tube eccentricity is calculated iteratively by using catenary as the initial state of the structure. Following the main tube eccentricity iteration process illustrated in Figure 4, the maximum main tube eccentricity $E(Z')$ of the truss arch elements of the bridge at the end of each iteration can be obtained. The admissible value of main tube eccentricity of all truss sections of the Bosideng Yangtze River Bridge is assumed to be 15.00 mm. The iteration results of main tube eccentricity are shown in Table 1 and Figures 7 and 8. After the 15th external cycle iteration, the maximum main tube eccentricity $E(Z'_*)$ is less than the admissible value of 15.00 mm, thereby satisfying the engineering accuracy requirements.

As can be seen from the charts above, the maximum main tube eccentricity of the Bosideng Yangtze River Bridge decreases from 63.23 mm to 14.91 mm after 15 external cycle iterations of the finite element model. Moreover, the maximum bending moment of the main tube decreases by 517.13% from 521.53 kN·m to 100.85 kN·m. The bending moment of each key section of the Bosideng Yangtze River Bridge is controlled within 100 kN·m, thereby highlighting the remarkable effect of iterative calculation.

3.3. Calculation of the Cubic Spline Interpolation Function. The cubic spline interpolation function is calculated by taking the final model of the iteration calculation of main tube eccentricity as the initial structure. Six key sections, namely, the arch foot section, border of the arch girder section, L/8, L/4, 3L/8, and midspan section, are selected as the control sections of the cubic spline interpolation function. The centroid coordinates of these sections are extracted from the finite element model and presented in Table 2.

According to the structural form of the Bosideng Yangtze River Bridge, the first boundary condition is selected as an additional condition of the cubic spline curve. The angles of the arch foot and midspan sections are $\alpha_1 = 44.35$ and $\alpha_6 = 0$, respectively, according to formula (15).

$$\begin{cases} S'(x_1) = f'(x_1) = \tan(44.35^\circ) = 0.976, \\ S'(x_n) = f'(x_n) = 0. \end{cases} \tag{27}$$

The coefficient matrix A of the spline curve is obtained as

$$A = \begin{pmatrix} 1.15e-4 & 7.83e-2 & 1.85e+1 & 1.42e+3 \\ -1.14e-5 & -8.4e-3 & -1.30e+0 & -7.95e+1 \\ 4.67e-6 & 2.00e-4 & 2.41e-1 & 1.21e+1 \\ 3.26e-8 & -1.59e-3 & 1.06e-2 & 2.21e+0 \\ -8.24e-7 & -1.76e-3 & -1.39e-17 & 1.98e+0 \end{pmatrix}. \tag{28}$$

The cubic spline curve of the half-bridge of the Bosideng Yangtze River Bridge is obtained based on the coefficient matrix A of the spline curve as shown in Figure 9.

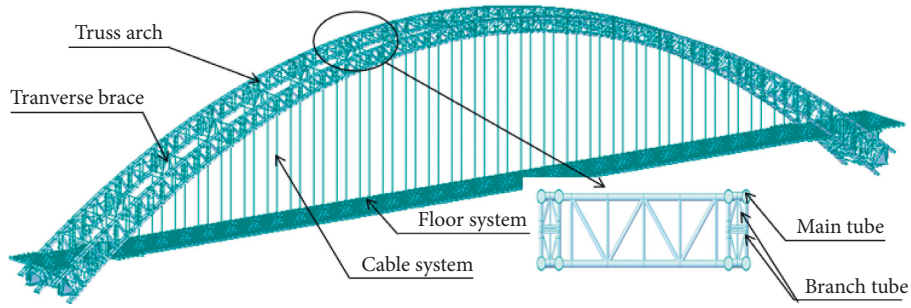

Figure 6: Bosideng Yangtze River Bridge and its elements.

Table 1: Iterative calculation of main tube eccentricity.

Number of iterations	E_a (mm)	E (mm)	Max-My (kN·m)
0	15.00	63.23	521.53
1	15.00	49.76	365.30
2	15.00	41.88	353.89
3	15.00	37.14	359.23
4	15.00	31.51	303.95
5	15.00	30.39	261.61
6	15.00	25.33	205.62
7	15.00	22.11	141.47
8	15.00	19.99	126.38
9	15.00	19.74	113.78
10	15.00	17.87	115.00
11	15.00	16.58	113.80
12	15.00	16.23	112.83
13	15.00	15.53	112.65
14	15.00	15.26	99.44
15	15.00	14.91	100.85

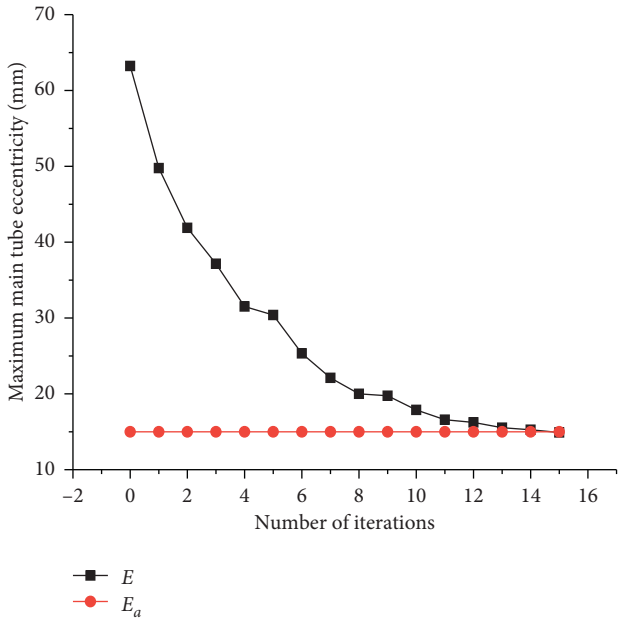

Figure 7: Maximum main tube eccentricity.

After calculating the coefficient matrix A of the spline curve, the $[X, Z]$ coordinate of each node of the truss arch can be calculated by using the parametric coordinates.

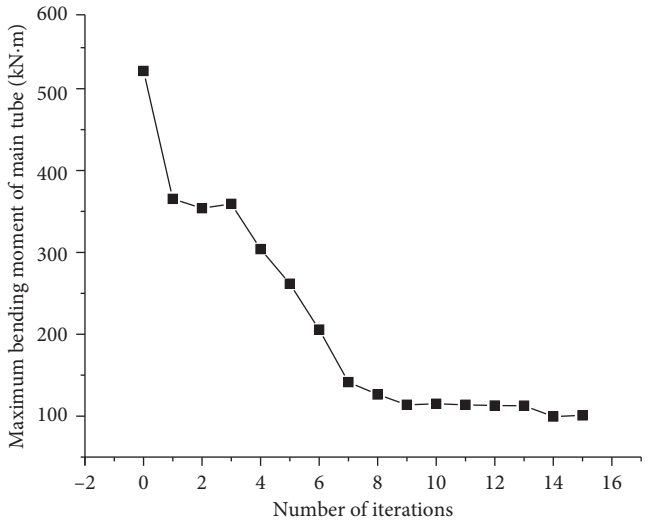

Figure 8: Maximum bending moment of the main tube.

Afterward, the structure state optimized by the cubic spline interpolation function is generated by importing the obtained coordinates into the finite element model of the Bosideng Yangtze River Bridge.

3.4. Analysis and Comparison of Internal Forces before and after the Optimization. By using main tubes 1 (upper chord) and 2 (lower chord) as examples, the internal force state of each key section of the Bodiseng Yangtze River Bridge is analyzed by comparing three types of optimal arch axis lines specific to this bridge, namely, the arch axis line type optimized by a parabola with an exponent of 2.1, the catenary with an arch axis coefficient of 1.35, and the cubic spline curve of coefficient matrix A, as shown in Figure 10.

As indicated by the maximum bending moment of the upper and lower chords of each key section, the parabola, catenary, and cubic spline curve have maximum bending moments of 546.65, 455.39, and 233.40 kN·m, respectively.

The curve of the cubic spline interpolation function is better than those of the parabola and catenary. The bending moment values of the six key sections of the cubic spline curve at the arch foot, border of the arch girder, L/4, 3L/8, and midspan significantly decrease. The L/8 span has slightly large bending moment values yet the bending moment at the section location is small, thereby highlighting the

Table 2: Centroid coordinates of the six key sections.

Centroid coordinates	Arch foot	Border of arch girder	L/8 span	L/4 span	3L/8 span	Midspan
X	−251.22	−228.05	−178.75	−128.70	−64.35	0.00
Z	−105.34	−85.93	−51.27	−25.57	−5.07	1.98

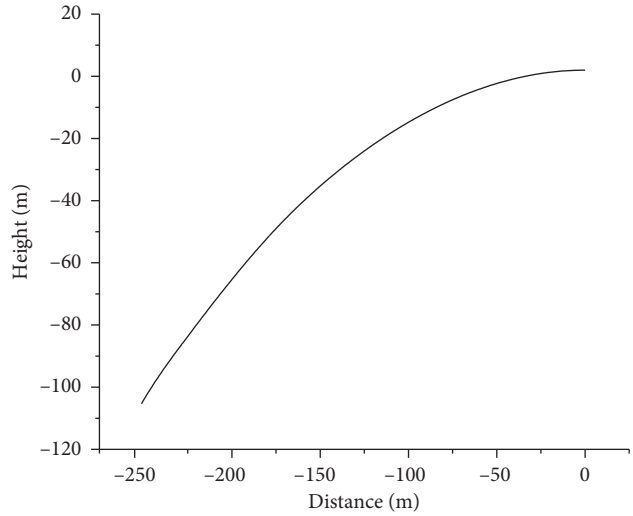

Figure 9: Half-span arch axis fitted by the cubic spline curve.

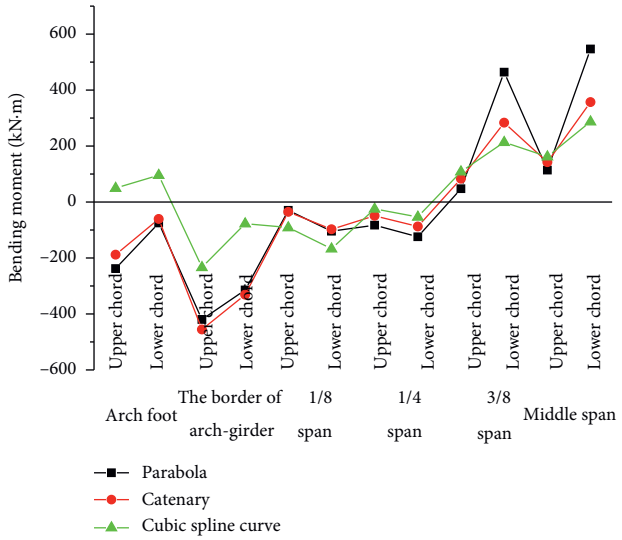

Figure 10: Bending moment of the six key sections.

remarkable optimization effect of the internal force state of the main arch rib.

3.5. Analysis and Comparison of the Mechanical Properties of the Finished Bridge State

3.5.1. Contrast of the Strength Index. Considering the self-weight and moving load of the structure, the maximum absolute stress of the upper and lower chords of the three optimal arch axis line types is calculated and compared under the basic load combination of the ultimate limit state according to formula (29) and as shown in Figure 11:

$$S_{ud} = 1.1 \times [1.2 \times (\text{the self} - \text{weight road}) + 1.4 \times (\text{the moving road})]. \quad (29)$$

Figure 8 shows that the maximum absolute stress of the upper and lower chords follows the same variation trend along the bridge span direction, but the stress amplitude of the cubic spline curve is smaller than that of the other curves. A high stress of lower than 100 MPa is only observed at the midspan of the lower chord.

3.5.2. Contrast of the Stiffness Index. The maximum vertical deflection (i.e., sum of the absolute values of maximum positive and negative deflection) under the lane load (excluding the impact coefficient) and the deflection curves of the upper and lower chords of the main arch rib are presented in Figure 12.

Figure 12 shows that the maximum vertical deflection of the cubic spline curve at the midspan is larger than that of the two other curves and that only a small difference is observed among the three curves at other positions, thereby proving that optimizing the main arch rib enhances the integral structure stiffness, but such effect is not obvious.

3.5.3. Contrast of the Stability Index. In analyzing the elastic stability of the CFST arch rib, the load of the bridge deck

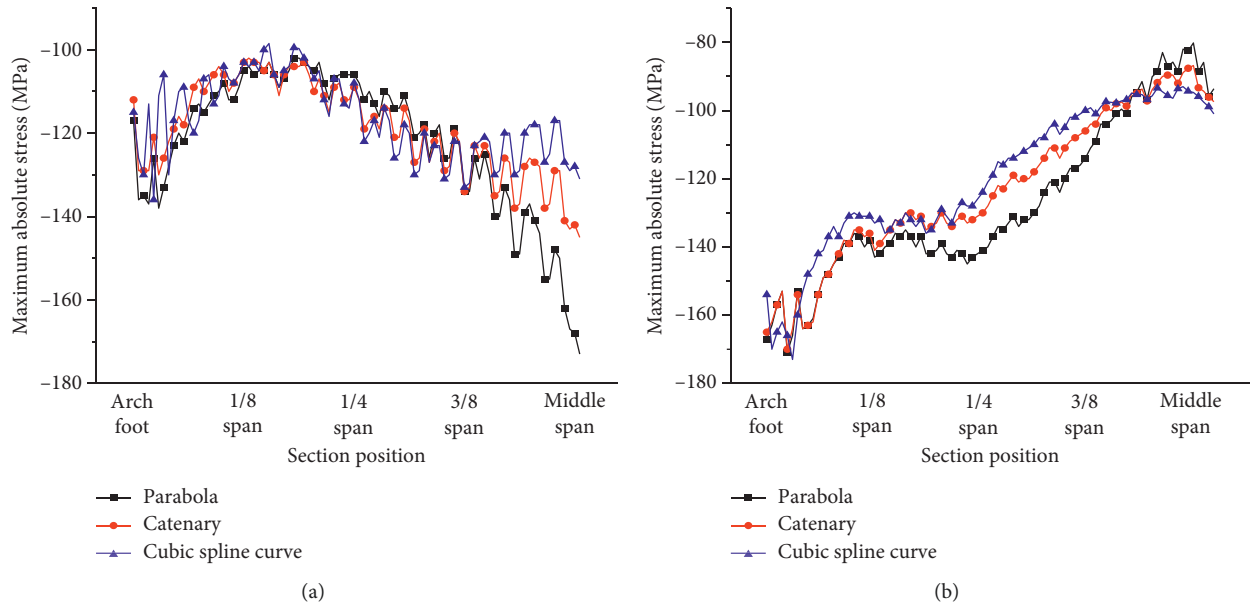

Figure 11: Stress distribution of the main arch rib of the half-bridge. (a) Stress distribution of the upper chord. (b) Stress distribution of the lower chord.

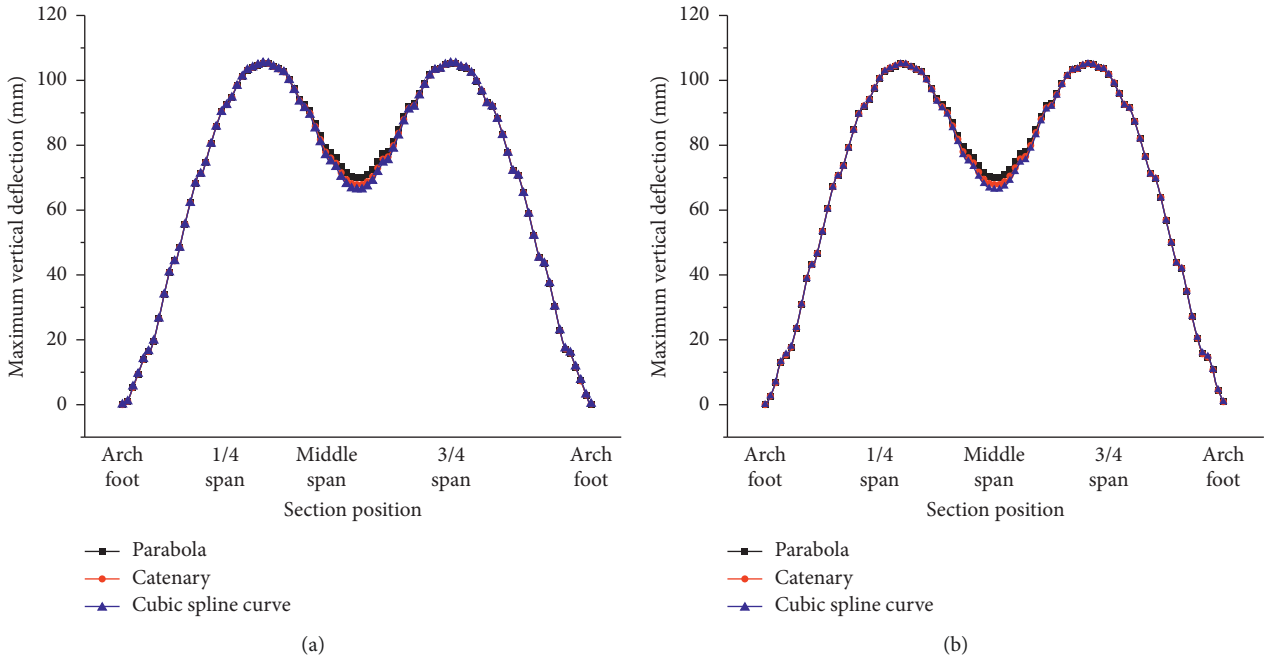

Figure 12: Deflection distribution of the main arch rib. (a) Deflection distribution of the upper chord. (b) Deflection distribution of the lower chord.

system, suspender weight, and moving load are all equivalent to the concentrated force of the top node of the suspender. The equivalent concentrated force of the moving load varies, whereas that of the other loads is invariant. A buckling analysis is conducted by using the Midas/Civil spatial finite element model. The results for the first four instability modes are shown in Figure 13.

As shown in the figure, the first four instabilities of the Bosideng Yangtze River Bridge are transverse. The elastic stability coefficient is shown in Table 3.

The stability coefficients of the three optimal arch axis line types progressively decrease from parabola and catenary to cubic spline curve at any order, thereby proving that the cubic spline curve has a better stability than the other two curves.

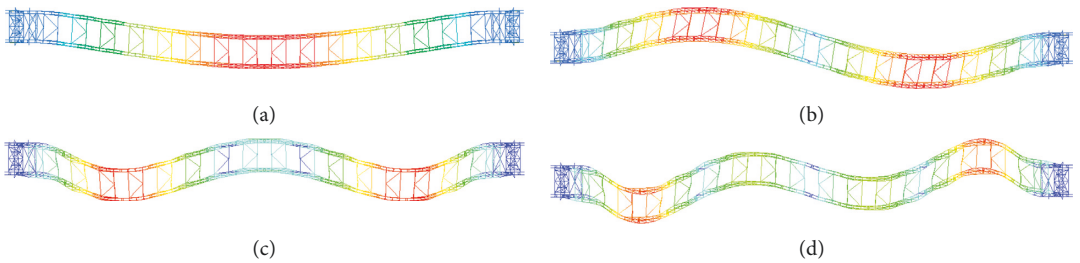

Figure 13: First four instability modes. (a) First-order instability mode. (b) Second-order instability mode. (c) Third-order instability mode. (d) Fourth-order instability mode.

Table 3: Stability coefficient of the first four instability modes.

Modal order	Instability mode	Parabola	Catenary	Spline curve
First mode	Symmetrical transverse	18.78	19.01	19.25
Second mode	Antisymmetrical transverse	22.15	22.73	22.84
Third mode	Symmetrical transverse	30.17	31.28	31.28
Fourth mode	Antisymmetrical transverse	35.55	35.74	35.92

4. Conclusions

The proposed minimum main tube eccentricity method considers the actual stress state of the main tube, effectively reduces its bending moment, and controls the maximum eccentricity to optimize the internal force state of the truss arch. This method is designed based on an iterative approach, which may not be the global optimum. Nevertheless, this approach increases the convergence of the algorithm and can be used to build an optimal solution that meets the engineering accuracy requirements. The iteration calculation is also convenient and efficient, thereby facilitating the optimization.

The proposed arch axis optimization method is applied by using the Bosideng Yangtze River Bridge as an example. The internal forces of three optimal arch axis line types are compared, and the findings indicate that the proposed method controls the eccentricity of the key sections, considerably reduces the bending moment of the main tubes, and ensures a uniform distribution of internal forces. Meanwhile, the analysis of the mechanical properties of the finished bridge state reveals that the stress amplitude of the cubic spline curve is smaller and more uniform than that of others, whereas its stiffness and stability are increased.

Data Availability

The testing and analysis data used to support the findings of this study are included in the article.

Conflicts of Interest

The authors declare no conflicts of interest regarding the publication of this paper.

Acknowledgments

This research was sponsored by the Construction Control Group of the Bosideng Yangtze River Bridge.

References

[1] B. C. Chen, "Application and research progress of concrete filled steel tubular arch bridge," *Highway*, vol. 11, pp. 57–66, 2008.

[2] B. C. Chen, "View and review of arch bridge technology," *Journal of Fuzhou University (Natural Science Edition)*, vol. 37, no. 1, pp. 94–106, 2009.

[3] B. C. Chen, J. W. Wei, J. Zhou, and J. P. Liu, "Application of concrete-filled steel tube arch bridges in China: current status and prospects," *China Civil Engineering Journal*, vol. 50, no. 6, pp. 50–61, 2017.

[4] J. L. Zhen, J. J. Wang, T. M. Mu et al., "Feasibility study on design and construction of concrete filled steel tubular arch bridge with a span of 700 m," *Strategic Study of CAE*, vol. 16, no. 8, pp. 33–37, 2014.

[5] B. C. Chen and Y. L. Yang, "Investigation and analysis of concrete-filled steel tube arch bridges," *World Bridges*, vol. 2, pp. 73–77, 2006.

[6] D. Bruno, P. Lonetti, and A. Pascuzzo, "An optimization model for the design of network arch bridges," *Computers & Structures*, vol. 170, pp. 13–25, 2016.

[7] M. H. Zhou, "Study on design of common arch axis curves," *Highway Engineering*, vol. 35, no. 3, pp. 92–95, 2010.

[8] Z. X. Liu, "The research on arch axial linetype of concrete filled steel tube (CFST) bridge," *Communications Standardization*, vol. 10, pp. 72–75, 2003.

[9] M. Y. Huang, "Reasonable form of concrete-filled steel tubular frame tied arch bridge," *Journal of Central South University of Forestry & Technology*, vol. 31, no. 2, pp. 90–94, 2011.

[10] Y. S. Zhao, *Design Optimization of Arch Rib Alignment of Concrete Filled Steel Tubular Arch Bridge*, Wuhan University of Technology, Hubei, China, 2007.

[11] N. Tong, *Study on Reasonable Arch axis of Long-Span Concrete Arch Bridge*, Chongqing Jiaotong University, Chongqing, China, 2013.

[12] T. J. Peng and D. Y. Yang, "Design and calculation analysis of flying bird concrete filled steel tubular arch bridge with reverse arch," *Journal of China & Foreign Highway*, vol. 36, no. 4, pp. 139–143, 2016.

[13] L. X. Liu and J. H. Gao, "Topkis-Veinott feasible direction method for optimum axis of arch bridge based on quartic spline function," *Journal of Highway and Transportation Research and Development*, vol. 24, no. 6, pp. 80–85, 2007.

[14] X. D. Jiang, X. S. Zhang, and Y. S. Zhao, "Linear optimization design of arch bridge and rib based on Matlab language," *Subgrade Engineering*, vol. 1, pp. 73–77, 2010.

[15] D. M. Peng and C. A. Fairfield, "Optimal design of arch bridges by integrating genetic algorithms and the mechanism method," *Engineering Structures*, vol. 21, no. 1, pp. 75–82, 1999.

[16] Y.-W. Dai and Y.-Y. Wang, "A research to cable force optimizing calculation of cablestayed arch bridge," *Procedia Engineering*, vol. 37, pp. 155–160, 2012.

[17] S. M. Zhou and Y. D. Li, "Weighted energy method for solving reasonable arch axes," *Journal of Highway and Transportation Research and Development*, vol. 27, no. 4, pp. 73–77, 2010.

[18] C. H. Hou and S. X. Song, "Research on the optimization of arch—axis and column layout based on APDL language," *Journal of Railway Engineering Society*, vol. 34, no. 10, pp. 55–59, 2017.

[19] Y. Xu and C. Y. Shen, "Analysis of optimizing internal force distribution of structural system of through tied-arch bridge," *Journal of Highway and Transportation Research and Development*, vol. 32, no. 12, pp. 67–74, 2015.

[20] Q. P. Jiang, "A study of method of determining rational arch axis using three order splin interpolation," *Journal o f Wuhan University of Technology (Transportation Science & Engineering)*, vol. 25, no. 1, pp. 101–104, 2001.

[21] N. B. Hao and A. B. Gu, "Construction control of 500 m concrete-filled cteel tubular arch bridge," *Journal of Southwest Jiaotong University*, vol. 50, no. 4, pp. 635–640, 2015.

[22] M. A. Latif and M. P. Saka, "Optimum design of tied-arch bridges under code requirements using enhanced artificial bee colony algorithm," *Advances in Engineering Software*, vol. 135, article 102685, 2019.

[23] P. Lonetti and A. Pascuzzo, "Design analysis of the optimum configuration of self-anchored cable-stayed suspension bridges," *Structural Engineering and Mechanics*, vol. 51, no. 5, pp. 847–866, 2014.

[24] P. Lonetti, A. Pascuzzo, and A. Davanzo, "Dynamic behavior of tied-arch bridges under the action of moving loads," *Mathematical Problems in Engineering*, vol. 2016, Article ID 2749720, 17 pages, 2016.

[25] J. Li, R. X. Zhang, and M. Jiang, "The optimum design of arch bridge axis based on Matlab," *Optimization of Capital Construction*, vol. 26, no. 3, pp. 68–70, 2005.

[26] W. He and C. X. Li, "Discussion on the unified mathematical description of arch axis-cubic NURBS representation," *Journal of China & Foreign Highway*, vol. 26, no. 6, pp. 137–140, 2006.

[27] N. Islam, S. Rana, R. Ahsan, and S. N. Ghani, "An optimized design of network arch bridge using global optimization algorithm," *Advances in Structural Engineering*, vol. 17, no. 2, pp. 197–210, 2014.

[28] H. J. Kang, W. D. Xie, and T. D. Guo, "Modeling and parametric analysis of arch bridge with transfer matrix method," *Applied Mathematical Modelling*, vol. 40, no. 23-24, pp. 10578–10595, 2016.

[29] Z. C. Tian, C. Sun, Y. H. Han, and G. T. Zhao, "Completed bridge suspender forces optimization of a arch bridge," *Journal of Railway Science and Engineering*, vol. 14, no. 2, pp. 296–302, 2017.

[30] J. F. He, Q. Fu, and H. D. Wang, "An improved simulated annealing algorithm for solving TSP," *Computer Era*, vol. 7, pp. 47–50, 2019.

[31] X. Gao, L. J. Wang, and Y. X. Du, "Structure reliability analysis by combining augmented multiplier method and simulated annealing algorithm," *Journal of Xi'an Jiao Tong University*, vol. 53, no. 11, pp. 144–152, 2019.

[32] R. F. Pu, "Improved simulated snnealing algorithm for global optimization problem of optimal solution," *Journal of Yibin University*, vol. 13, no. 6, pp. 78–81, 2013.